Modèle de Cox

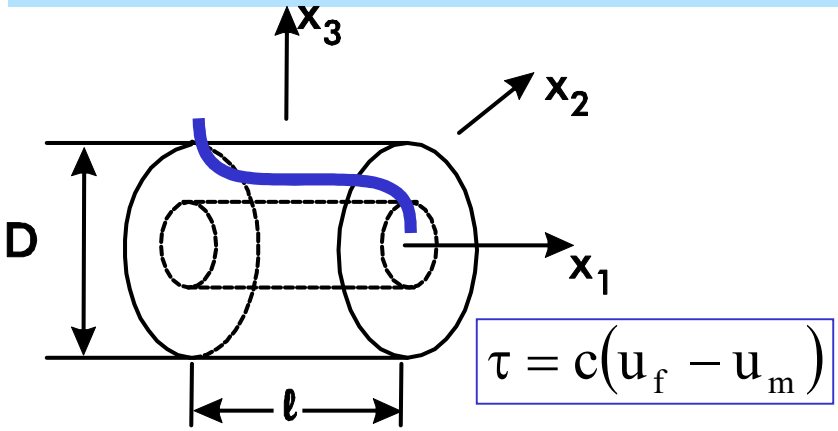

Stress-strain transfer in fibre systems, Cox 1952 (paper)
Elastic stress transfer at interfaces
Fragmentation test, pull out tests…
Laser Raman to measure local carbon-fibre strains…
Shift of atomic vibrational frequencies upon fibre strain
Elastic and frictional load transfer, Lévèque CSTE 1996

ELSEVIER
Composites Science and Technology
Volume 56, Issue 7, 1996, Pages 749-754

Study of carbon-fibre strain in model composites by raman spectroscopy

D. Lévêque *, M.-H. Auvray

coupons with the M40B fibre (M40B/LY B1 and M40B/LY C2) and one with the HMS fibre (HMS/LY

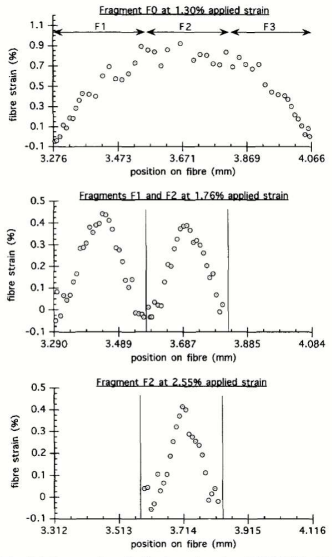

Fig. 4. Fibre strain distribution for the M40B/LY C2 specimen at increasing applied strain, ε_∞.

3 RESULTS AND DISCUSSION

3.1 Load-transfer mechanisms

Experimental strain profiles are fitted (Fig. 5) as follows:

1. A straight line for the debonded parts. We have to distinguish the fragment ends without strain on which the E_{2g} band position is nearly constant with an important background level probably due to fluorescence in the resin because of degradation near the fibre (local yield flow underlined by transmitted polarized light after unloading of the specimen),[7] from the parts loaded by friction (Fig. 5(a)) where the curve of strain versus position on the fibre is linear.
2. A Cox curve in the case of elastic load transfer (Fig. 5(a,b)). The strain is then expressed as:[8]

$$\varepsilon(x) = \varepsilon_m[1 - (ch(\beta l_e/2 - \beta(x - x_e))/ch(\beta l_e/2))] \quad (1)$$

where ε_m is the maximum strain at the top of the elastic stress transfer, l_e is the length of no debonded fragment, x is the position on the fibre, x_e is the position at the beginning of elastic load transfer, and β is the Cox parameter which depends on geometrical and mechanical parameters. Although varying during the test, the value of β is found to be close to the theoretical value.

Thus, we find a noticeable difference in behaviour between the HMS fibre which is nearly all debonded at the end of the fragmentation process and uses a friction transfer mechanism, and the M40B fibre whose debonding is more limited and without any friction.

3.2 Quantitative analysis

The interfacial shear stress is derived from the strain profiles by use of the force balance relationship around an infinitesimally small fibre element of length dx:

$$\tau(x) = (1/2)R_f E_f(d\varepsilon(x)/dx) \quad (2)$$

where R_f is the fibre radius and E_f the Young's modulus.

In the case of a pure elastic load transfer (eqn (1)), the shear stress is a maximum at the ends of this load transfer: $\tau_{max} = \tau_e(x = x_e)$. If the fragment is loaded only by friction acting on a length l_f: $\tau_{max} = \tau_f$. For a mixed load transfer, the mean shear stress value, τ_m^R, deducted from the Raman measurements on a fragment of length L is expressed by:

$$\tau_m^R = \left(2\int_{x_e}^{x_e + l_d/2} \tau_e(x)dx + \tau_f l_f\right)\Big/ L \quad (3)$$

Assuming a Coulomb friction state for the HMS/LY system then $\tau_f = \mu P$, where μ is the friction coefficient and P is the radial stress on the fibre calculated in a simply elastic bicylinder scheme; we find that the value of μ lies between 0·7 and 1·4.

For each profile fit for HM fibres, Tables 2 and 3 give the values of τ_{max} and τ_m^R, the cumulative number of ruptures, N_r, on the observation length, L_0, and the total debonded length, l_d ($= L - l_e$). Moreover, the values of l_c and τ_m^{K2} are calculated at the saturation level of the fragmentation process. It is very interesting to compare τ_m^R with τ_m^K since both mean stresses are reflecting the ability of the fibre/matrix system to transfer the load by shear. On the one hand these values are close together for the HMS/LY system which reaches essentially a state of frictional loading at the saturation level, as assumed in the Kelly model. On the other hand, τ_m^R is 30% lower than τ_m^K for the M40B fibre on which the load transfer remains only elastic. The maximum value of τ_{max} is an estimate (lower bound) of the interfacial shear strength: from 40 MPa for the HMS/LY system to 64 MPa for the M40B/LY system.

3.3 Residual thermal strain and evolution of the fibre strain

The evolution of the mean strain in the fibre measured before the first break as a function of the tensile strain, ε_∞, applied to the specimen is plotted in Fig. 6. This graph provides us with valuable information:

- When the specimen is not yet loaded $\varepsilon_\infty = 0\%$, the measured strain, corresponds to the residual thermal strain in the fibre. It is a compressive strain since the thermal expansion coefficient of the matrix is far greater than the longitudinal thermal expansion coefficient of the fibre. This residual strain is about −0·1%, much lower in absolute value than the −0·6% coming from a theoretical calculation.[6] This discrepancy may

EPFL pierre-etienne.bourban@epfl.ch

C_{ij} et E_i et Q_{ij}

$$\{\sigma\} = [C]\{\varepsilon\}$$

$$\begin{bmatrix}\sigma_1\\ \sigma_2\\ \sigma_3\\ \sigma_4\\ \sigma_5\\ \sigma_6\end{bmatrix} = \begin{bmatrix} C_{11} & C_{12} & C_{13} & C_{14} & C_{15} & C_{16}\\ C_{21} & C_{22} & C_{23} & C_{24} & C_{25} & C_{26}\\ C_{31} & C_{32} & C_{33} & C_{34} & C_{35} & C_{36}\\ C_{41} & C_{42} & C_{43} & C_{44} & C_{45} & C_{46}\\ C_{51} & C_{52} & C_{53} & C_{54} & C_{55} & C_{56}\\ C_{61} & C_{62} & C_{63} & C_{64} & C_{65} & C_{66}\end{bmatrix} \begin{bmatrix}\varepsilon_1\\ \varepsilon_2\\ \varepsilon_3\\ \varepsilon_4\\ \varepsilon_5\\ \varepsilon_6\end{bmatrix}$$

TMX15 … test A, contrainte uniaxiale

$$E_1 = C_{11} - \frac{2C_{12}^2}{C_{22} + C_{23}}$$

$$\{\varepsilon\} = [S]\{\sigma\}$$

$$[S_{ij}] = \begin{bmatrix} S_{11} & S_{12} & 0\\ S_{12} & S_{22} & 0\\ 0 & 0 & S_{66}\end{bmatrix} = \begin{bmatrix} 1/E_1 & -\nu_{21}/E_2 & 0\\ -\nu_{12}/E_1 & 1/E_2 & 0\\ 0 & 0 & 1/G_{12}\end{bmatrix}$$

Composites orthotropes en contraintes planes
Q_{ij}, rigidités réduites….seul C_{66}=Q_{66}

Slides Macromécanique et TMX

$$Q_{11} = \frac{E_1}{(1-\nu_{12}\nu_{21})}$$